Conformational Dynamics of a 5S rRNA Hairpin Domain Containing Loop D and a Single Nucleotide Bulge

Joanna Sarzynska,*† Tadeusz Kulinski,† and Lennart Nilsson*
*Center for Structural Biochemistry, Department of Bioscience at NOVUM, Karolinska Institutet, SE-141 57 Huddinge, Sweden; and †Institute of Bioorganic Chemistry, Polish Academy of Sciences, 61 704 Poznan, Poland

ABSTRACT Molecular modeling and molecular dynamics have been employed to study the conformation and flexibility of a 15-nucleotide fragment of the plant 5S rRNA containing loop D and a single uridine bulge. Two different model built initial structures were used: one with the bulge localized inside the helical stem and another with the bulge pointing out from the helix. Several independent 700-ps-long trajectories in aqueous solution with Na^+ conterions were produced for each starting structure. The bulge nucleotide inside the helix stayed in two main conformations, both of which affected the geometry of the stem part opposite the bulge. When the bulge nucleotide was located outside the helix, we found high base mobility and local backbone flexibility. The dynamics of the hydrogen bond network and conformational changes from a direct to a water mediated hydrogen bond in the sheared G-A basepair in the tetraloop was described. Our results correlate with lead ion induced cleavage patterns in 5S rRNA. Sites resistant to nonspecific lead cleavage appeared in all our simulations as the most rigid fragments independent of the localization of the bulge nucleotide.

INTRODUCTION

5S Ribosomal RNA is an integral component of the large subunit of both prokaryotic and eukaryotic ribosomes. This rRNA, about 120 nucleotides long, has been the subject of various studies concerning its structure and biological function. A general secondary structure of prokaryotic and eukaryotic 5S rRNA was proposed on the basis of sequence alignments and available biochemical data (Specht et al., 1990). A large amount of sequence data for molecules of different origin has been collected and is deposited in the 5S Ribosomal RNA Data Bank (Szymanski et al., 1999). The consensus secondary structure of all 5S rRNAs possesses a three-way junction with three arms containing helical regions (I-V) and internal loops (B, E). Hairpins with loops C and D terminate two of those arms. (In the literature we have found different notations for the regions of 5S rRNA. In this paper, helices are designated by roman numerals I-V and loops by capital letters A-E; Szymanski et al., 1999). The tertiary structure of 5S rRNA is not fully known, and details of the secondary structures for particular molecules still remain a matter of discussion. Significant contributions toward understanding 5S rRNA structure in solution come from biochemical methods such as enzymatic digestion, chemical modification, oligonucleotide binding, or metal ions hydrolysis.

Several attempts have been made to crystallize the whole 5S rRNA molecule, but the obtained crystals are not suitable for structure determination at atomic resolution (Lorentz et al., 1991). At present the tertiary structures are known for parts of the molecule, corresponding to the two arms of the prokaryotic 5S rRNA. Solution structures have been obtained for an *Escherichia coli* 5S rRNA fragment containing an internal loop E terminated by loop D (Dallas and Moore, 1997) and for the loop E region in complex with the ribosomal protein L25 (Stoldt et al., 1999). Crystal structures encompassing helix I and loop E-helix IV of *E. coli* 5S rRNA (Correll et al., 1997), helix I and helix IV terminated by a tetraloop of *Thermus flavus* 5S rRNA (Betzel et al., 1994; Perbant et al., 1998) are also available. For eukaryotic 5S rRNA the only known structure is that in solution containing the internal loop E (Wimberly et al., 1993). The recent successful determination of the crystal structure of the large and small ribosomal subunits at 5 Å and 5.5 Å resolution, respectively, brought again an interest in determining the structural details and interactions of the components of large structures (Ban et al., 1999; Clemons et al., 1999).

The subject of this study is a fragment of plant 5S rRNA from wheat germ and lupin seeds corresponding to the natural sequence of nucleotides 81 to 95 of helix IV - loop D (Fig. 1).

Helix IV of the eukaryotic 5S rRNAs, in contrast to the bacterial ones, contains a single nucleotide bulge in the 5′ strand. For plant 5S rRNA an alternative model was proposed where an enlarged loop D encompasses nucleotides 84–92 and is involved in tertiary interactions (Joachimiak et al., 1990). Analysis of the lead ion induced cleavage patterns suggested that the presence of the bulge nucleotide U84 destabilizes two potential basepairs, G85-C91 and G86-C92, at the bottom of helix IV and causes an enlargement of loop D (Ciesiolka and Krzyzosiak, 1996), but tertiary interactions were not confirmed. Additionally, the cleavage pattern for this fragment of RNA from plants is clearly different from that for other studied tetraloops in the GNRA family (N is any nucleotide, R is purine; Ciesiolka et

Received for publication 22 March 2000 and in final form 31 May 2000.
Address reprint requests to Lennart Nilsson, Center for Structural Biochemistry, Department of Bioscience at NOVUM, Karolinska Institutet, Hälsovägen 7, SE-141 57 Huddinge, Sweden. Tel.: 46-8-6089228, Fax: 46-8-6089290; E-mail: Lennart.Nilsson@biosci.ki.se.

0006-3495/00/09/1213/15 $2.00

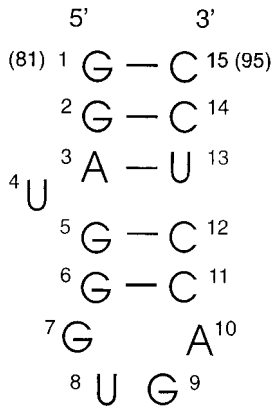

FIGURE 1 Secondary structure of the 5S rRNA fragment containing part of the helix IV and the loop D (which corresponds to the nucleotides 81–95 of the 5S rRNA from lupin seeds and wheat germ) according to Kulinski et al. (1997).

al., 1998). However, this fragment itself exhibits high thermodynamic stability. A model consistent with structural transitions observed calorimetrically, postulates the existence of a basepaired helical region, G85-G86:C92-C91, and a structured tetraloop, GUGA (Kulinski et al., 1997). Therefore, knowledge of the potential conformational dynamics of this RNA fragment may bring us closer to the understanding of RNA folding and its propensity for intra- and intermolecular interactions.

The aim of this study is to analyze the structural details of plant 5S rRNA fragment (nucleotides 81–95) and its conformational equilibrium in aqueous solution by molecular modeling and molecular dynamics (MD) simulation. The structural diversity obtained from several 0.7-ns-long MD trajectories provides an estimate of the range and stability of possible internal interactions and stabilizing role of water molecules within this RNA structural motif.

METHODS

Two different initial structures were used for the MD simulations. For each structure two independent, 700-ps-long simulations that differ in the initial velocities were performed (see Table 1). Simulations were run with periodic boundary conditions (PBC). To reduce the number of water molecules in the system and to compare the influence of the boundary condition on the results, for one initial structure we have also performed simulations with stochastic deformable boundary conditions (SDB; Brooks and Karplus, 1983). MD simulations and all calculations were performed with the CHARMM program version 25a2 and 26a2 (Brooks et al., 1983) using the force field version 22 (MacKerell et al., 1995).

Simulation protocol

Initial structures

For the investigation of the GGA*UGGGUGA*CCUCC RNA oligomer forming a hairpin with a GUGA tetraloop and a single uridine bulge (underlined; Fig. 1), two initial structures were built: one with the bulge located inside the helix (*bulge_in*) and another with the bulge outside the helix (*bulge_out*).

TABLE 1 Simulations presented in this work and the average RMS deviations from the initial structures

Simulation	RMS (Å)		Structural type
	Whole molecule (last 200 ps of MD)	Tetraloop (700 ps of MD)	
Initial structure *bulge_in*			
MD in a water box			
Sb1	2.2 (0.2)	1.3 (0.2)	*bul_in_1*
Sb2	2.1 (0.2)	1.0 (0.1)	*bul_in_2*
MD in a water sphere			
Ss3	2.3 (0.1)	1.3 (0.2)	*bul_in_1*
Ss4	2.2 (0.2)	1.5 (0.2)	*bul_in_1*
Ss5	2.0 (0.2)	1.2 (0.2)	*bul_in_2*
Ss6	3.0 (0.2)	1.0 (0.1)	*bul_in_2*
Initial structure *bulge_out*			
MD in a water box			
Sb7	1.9 (0.2)	1.6 (0.2)	*bul_out*
Sb8	2.0 (0.2)	1.6 (0.2)	*bul_out*

All simulations are 700 ps long. Values in parentheses are standard deviations.

In both structures the loop part was derived from the NMR structure for the GGGC*GAGA*GCCU RNA hairpin loop containing a GAGA tetraloop (PDB code 1zig; Jucker et al., 1996). To get a GUGA tetraloop, in the GAGA tetraloop the adenine base (A) was changed manually to a uracil base (U).

Initial structure bulge_in

First a 16-nucleotide hairpin was built. The geometry of the 4-bp stem fragment (nucleotides 1–4 and 12–15) was derived from the coordinates of canonical A-RNA (Arnott et al., 1976). The stem-loop part (nucleotides 5–12) came from the nuclear magnetic resonance (NMR) structure for the hairpin containing GAGA tetraloop, and in this part, two bases adjacent to the tetraloop were manually changed (C to G and G to C). Then 100 steps of steepest descent (SD) energy minimization were applied. To create a 15-mer with the U bulge in position 4, the base-pairing nucleotide A from the opposite strand was removed and 2500 steps of SD minimization were applied.

Initial structure bulge_out

The 2-bp stem part (nucleotides 1–2 and 14–15) came from the standard A-RNA form. The bulge region was derived from the x-ray structure for an RNA bacteriophage coat protein-operator complex (PDB code 1zdh; Valegård et al., 1997). Coordinates for nucleotides 3–6 and 11–13 were taken from the 5′G*A*GG/5′CCC stem part containing a single bulged nucleotide (underlined) of the RNA hairpin. In this part, three bases were manually changed (the bulge base A to U and the 5′ adjacent basepair G-C to A-U). The loop part (nucleotides 7–10) came from the NMR GAGA tetraloop structure. Finally, the structure was minimized with 100 steps of SD.

All energy minimizations during the initial structure building were done using harmonic restraints with a 10.0 kcal·mol^{-1}·Å^{-2} force constant on all atoms.

For both structures, 14 Na^+ counterions were placed on the bisector of the phosphate oxygen atoms, 6.0 Å from the phosphorus atoms. The whole

system was solvated in a 45 × 35 × 35 Å size water box (*bulge_in, bulge_out*) or in a water sphere (R = 23 Å; *bulge_in*) containing TIP3P water (Jorgensen et al., 1983). Water molecules <2.0 Å from RNA or Na^+ were removed. The resulting system contained a total of 1606 water molecules in the box and 1398 water molecules in the sphere, corresponding to RNA concentrations of 30 and 32 mM and ion concentrations of 0.42 and 0.46 M Na^+ in the box and the sphere, respectively. The center of the water sphere was set on the atom N4(C11). Energy minimization by 100 steps of SD without any restraints was applied to the solvated system.

Simulations were run with time step 0.002 ps and the SHAKE algorithm was used to constrain all bonds to hydrogens (Ryckaert et al., 1977). Coordinates were saved every 100 steps. The nonbonded interaction energies and forces were smoothly shifted to zero at a cutoff of 12.0 Å by the atom-based truncation method with a force-shifting function (Steinbach and Brooks, 1994). The nonbonded pair list was regenerated for atoms within a 13.0-Å cutoff on average every 5 steps, but every 10 steps for simulations Sb2 and Sb7, and every 20 steps for simulations simulation Sb1. (For a notation of the simulations, see Table 1.) The relative dielectric constant was set to 1.0. Extensive simulations of DNA duplexes have shown this protocol to yield trajectories that are very similar to trajectories obtained using Ewald summation, in terms of both structural stability and flexibility (Norberg and Nilsson, 2000).

For MD simulations with stochastic boundary conditions (Brooks and Karplus, 1983) the Langevin dynamics algorithm with a friction coefficient 50.0 ps^{-1} for the water oxygen atoms in the buffer region between R = 21 Å and R = 23 Å was applied.

Simulations were performed in the microcanonical ensemble and the temperature was periodically checked and kept within the window 300 ± 10 K.

In simulations with PBC, the entire system, with no restraints, was heated from 50 K to 300 K over 6 ps. The temperature was progressively increased by velocity scaling in steps of 50 K with 1 ps of MD at each step. The simulations were continued to 700 ps and the trajectories were saved for analysis. The initial 100 ps of the trajectories was considered an equilibration period and the analyses of simulations were performed on the next 600 ps of the production trajectory. Only data concerning RMSD (Table 1 and Fig. 2) and hydrogen bonds in the tetraloop (Table 5 and Fig. 7) come from the analysis of the full 700-ps-long trajectory. Illustrations of structures and structural motifs were made with the program MolScript (Kraulis, 1991).

RESULTS

We have performed several molecular dynamics simulations of a 15-nucleotide RNA structure containing a tetraloop and a single nucleotide bulge in the stem part, in aqueous solution with sodium counterions. Two different models of the bulge location were used. Initial structures were built using both NMR and x-ray derived coordinates for the RNA motifs. The loop part in both structures was similar, but the structures differed in the bulge region. In one initial structure the bulge nucleotide was inside (*bulge_in*), and in the other it was outside the helix (*bulge_out*).

For the initial structure *bulge_in*, two independent simulations in a water box were performed (Sb1, Sb2). Simulations in the water box were compared with simulations in a water sphere (Ss3, Ss4, Ss5, Ss6). Two independent simulations, starting from the initial structure *bulge*_out, were run in the water box (Sb7, Sb8). All simulations are 700 ps long (Table 1).

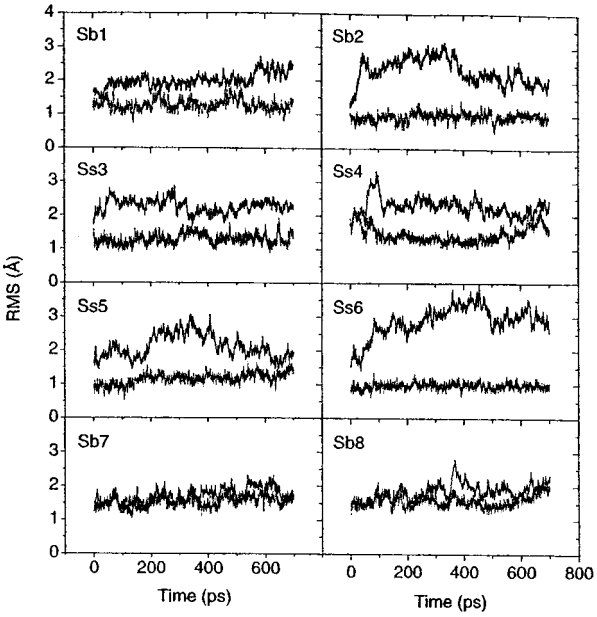

FIGURE 2 Root mean square (RMS) deviation compared to the initial structures, whole molecule (*solid line*) and tetraloop (nucleotides 7–10; *dashed line*). Simulations Sb1, Sb2 (in the water box), Ss3, Ss4, Ss5, and Ss6 (in the water sphere) start from the initial structure *bulge_in*. Simulations Sb7 and Sb8 (in the water box) start from the initial structure *bulge_out*.

Structural stability

We obtained stable trajectories both in the water box and in the water sphere without any systematic drift of the root mean square deviation (RMSD) from the initial structure (Fig. 2). The average global RMSD over the last 200 ps of MD was in the range 1.9–2.3 Å with one exception, in the simulation Ss6, where the final value was around 3.0 Å (Table 1). In all simulations the tetraloop part remained close to the initial structure, with an RMSD in the range 1.0–1.6 Å. Trajectories Sb2 and Ss6 showed the lowest and most stable RMSD for the tetraloop. As we will see later, in these cases we did not observe formation of a water-mediated hydrogen bond between bases G7 and A10.

Structural diversity

As a result of starting simulations from two initial structures and running several independent molecular dynamics trajectories for each of them, we obtained different possible conformations of the system. Details of the structures in the bulge region will be analyzed separately for simulations starting from initial structure *bulge_in* and *bulge_out*, whereas the tetraloop conformation which was similar for both initial structures, will be discussed for all simulations together.

Bulge region

To describe structures obtained from simulations starting from the initial structure *bulge_in* in the bulge region, particularly the orientation of the bulge base, we calculated distances between the N1 atom of the bulge uracil (U4) base and the N9 atom of adjacent bases: adenine (A3) and guanine (G5; Fig. 3 *A*).

Structures in the bulge region can be divided into two groups according to the distances between those nitrogens. One group (*bul_in_1*) represents structures where U4 is closer to G5 with the distance between N9(A3) and N1(U4) in the range 6.4–6.6 Å and the distance between N1(U4) and N9(G5) in the range 4.8–5.0 Å. The second group (*bul_in_2*) contains structures where U4 is closer to A3 with the distance between N9(A3) and N1(U4) in the range 4.5–4.9 Å and the distance between N1(U4) and N9(G5) in the range 5.8–6.0 Å.

In the structures belonging to the group *bul_in_1* (simulations Sb1, Ss3, Ss4), the bulge nucleotide U4 is somewhat outside the helix in the minor groove side and the base is not exactly parallel to the neighboring adenine and guanine bases. The average angles between normal vectors of the bulge uracil base and adjacent adenine or guanine bases are similar and in the range of 25–33° (Fig. 3 *B*). The uracil base remains in close contact with the flanking adenosine base: (U4)O4. . .H-C2(A3) (Table 2 and Fig. 4 *A*). For this group of structures there is also a hydrogen bond (A3)O2′-H. . .O5′(U4) (Table 4).

In the structures from the group *bulge_in_2* (simulations Sb2, Ss5, Ss6), the bulge nucleotide U4 stays stacked with A3 and a bend between U4 and G5 is observed (Fig. 4 *B*). The angle between the normal vectors of U4 and G5 is in the range 68–78° (Fig. 3 *B*). The bulge uracil base is hydrogen bonded with O_2(U13) or O6(G5). Hydrogen bonds (A3)O2′-H. . .O4′(U4) or (C12)O2′-H. . .O5′(U13) along the backbone are found for two simulations, Sb2 and Ss5 (Table 4).

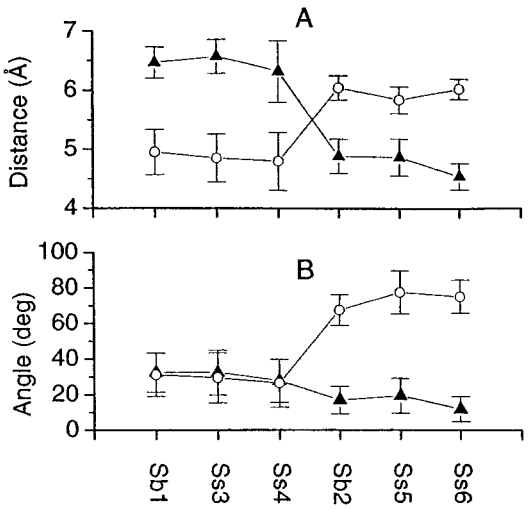

FIGURE 3 The orientation of the bulge uracil base U4 with respect to the flanking basepairs in six simulations started from the initial structure *bulge_in*. (*A*) Average distances between the N1 atom of the bulge uracil base (U4) and the N9 atom of adjacent bases: adenine (A3, *triangles*) and guanine (G5, *circles*). (*B*) Average angles between normal vectors of the uracil base and the adjacent bases: adenine (A3, *triangles*) and guanine (G5, *circles*).

Structures obtained from the simulations starting from initial structure *bulge_out* (simulations Sb7, Sb8) do not represent a single well-defined conformation in the bulge region. The position of the bulge nucleotide both differs between simulations and changes along them. With the bulge base on the outside of the helix, stacking of the flanking bases A3 and G5 on each other is possible, and also occurs most of the simulation time. The bulge uracil base is not involved in any direct hydrogen bonds or stacking interaction. Differences in the position of the bulge phosphate group and the bulge base relative to the helix can be seen from the superposition of the two final structures (averaged over the last 20 ps of MD) obtained from simulations Sb7 and Sb8 (Fig. 5 *C*). Hydrogen bonds involving the 2′OH group of nucleosides G2, A3, U4 are found over the whole trajectories or only during part of simulations (Table 4).

The Watson-Crick basepairs flanking the bulge were maintained for most of the simulation time (Table 2). A few reversible breakings of the hydrogen bonds were observed in the minor grove side of these basepairs for the simulations *bulge_in*. Two reversible breaking events took place for the hydrogen bond N1. . .H-N3 of basepair A3-U13 (Ss4, Ss6). The base-pairing distortion observed in the simulation Ss6 was connected with rotation of the χ13 glycosyl torsion angle from anti toward the high anti (-sc) conformational region. For the simulations from the group *bulge_in_1*, the relative orientation of the A3 and U13 bases is similar to the U4 and U13 (range 23°–30°; Table 3). For the G5-C12 basepair, breaking of the N2-H. . .O_2 and partially of the N1-H. . .N3 hydrogen bond was observed during the simulation Ss6. For this simulation the G5-C12 basepair has a less optimal geometry due to the (U4)N3-H. . .O6(G6) hydrogen bond between the bulge base and the subsequent base in the strand (Table 2). The G5-C12 basepair is not planar and the angle between normal vectors of the G5-C12 oscillates around 41°; the N4-H. . .O4 (G5-C12) hydrogen bond also displays high fluctuations over the whole trajectory.

Hydrogen bond system in the loop

The tetraloop contains a sheared G-A basepair. There are up to four hydrogen bonds between G7-A10 and additional hydrogen bonds between O_2'-H of G7 and N7 of G9 (Fig. 5 *A*). For most of the simulations (6 out of 8) the average distance between N3(G7) and H6-H (A10) is in the range 4.6–4.8 Å, which is too long for a standard hydrogen bond (Table 5). In these cases we found a water bridge between N3(G7), N6-H(A10), and N7(G9) created by a single water

TABLE 2 Hydrogen bond geometry of the bulge region

	Watson-Crick basepairs					Bulge base		
	A3-U13		G5-C12			U4-U13	U4-G5	U4-A3
	N6-H . . . O4	N1 . . . H-N3	N2-H . . . O2	N1-H . . . N3	O6 . . . H-N4	N3-H . . . O2	N3-H . . . O6	O4 . . . H-C2
Sb1	1.99 (0.23)	1.99 (0.16)	2.04 (0.21)	2.07 (0.13)	1.94 (0.17)			2.51 (0.23)
	160 (12)	163 (9)	162 (9)	162 (10)	162 (10)			137 (12)
Ss3	2.08 (0.25)	1.94 (0.14)	1.95 (0.16)	2.05 (0.12)	2.00 (0.20)			2.58 (0.27)
	158 (12)	163 (9)	163 (9)	160 (10)	159 (10)			133 (15)
Ss4	2.04 (0.27)	2.11 (0.39)	1.99 (0.17)	2.05 (0.12)	1.93 (0.17)			2.68 (0.52)
	159 (13)	157 (16)	162 (9)	163 (9)	162 (11)			121 (25)
Sb2	2.04 (0.30)	2.09 (0.24)	2.02 (0.20)	2.10 (0.14)	2.09 (0.24)	2.09 (0.35)		
	162 (10)	155 (16)	160 (10)	154 (10)	149 (14)	151 (16)		
Ss5	1.98 (0.25)	1.99 (0.15)	2.05 (0.23)	2.12 (0.16)	2.10 (0.25)	2.27 (0.46)		
	161 (12)	164 (9)	159 (11)	153 (10)	148 (14)	150 (16)		
Ss6	1.96 (0.20)	2.41 (0.81)	2.32 (0.61)	2.24 (0.28)	2.60 (0.43)		2.04 (0.22)	
	163 (10)	146 (25)	148 (17)	151 (11)	127 (18)		146 (14)	
Sb7	2.04 (0.23)	1.92 (0.12)	1.94 (0.16)	2.04 (0.12)	2.04 (0.22)			
	163 (10)	165 (8)	161 (10)	165 (8)	160 (12)			
Sb8	1.94 (0.18)	1.94 (0.11)	1.95 (0.16)	2.05 (0.11)	2.01 (0.19)			
	164 (9)	166 (8)	163 (9)	165 (8)	162 (10)			

Average distances and angle values are in angstroms and degrees, respectively. RMS fluctuations are given in parentheses.

molecule (Fig. 6 *A*). This bridging water molecule was exchanged relatively slowly. For five simulations, we found the same water molecule in the bridge position for more than 400 ps. Dynamically stable tetraloop configurations with a direct hydrogen bond N3(G7) to N6 (A10), without water bridges in the loop, were also observed in the course of two 700-ps-long simulations, Sb2 and Ss6. (Fig. 6 *B*). During one simulation, Ss5, we observed a change of the loop arrangement and creation of water bridges (Fig. 7). The rearrangement to a direct hydrogen bond (G7)N3. . .H-N6(A10) from a water-mediated hydrogen bond was not observed.

For the structures with water bridges between bases in the loop (Sb1, Ss3, Ss4, Ss5b, Sb7, Sb8), average distances and angles of the (G7)N2-H. . .N7(A10) hydrogen bond are in the range 2.33 Å to 2.63 Å and 139° to 144°, respectively (Table 5). We found a stronger hydrogen bond between the N2 amino proton of G7 and the phosphate oxygen of A10: (G7)N2-H. . .O1P(A10). There is also a hydrogen bond between the N1 imino proton of G7 and the phosphate oxygen of A10: (G7)N1-H. . .O1P(A10), although its geometry in some cases is less optimal. The hydrogen bond (G7)O2′-H. . .N7(G9) in some simulations displays breaking events. For the structures without the water bridges

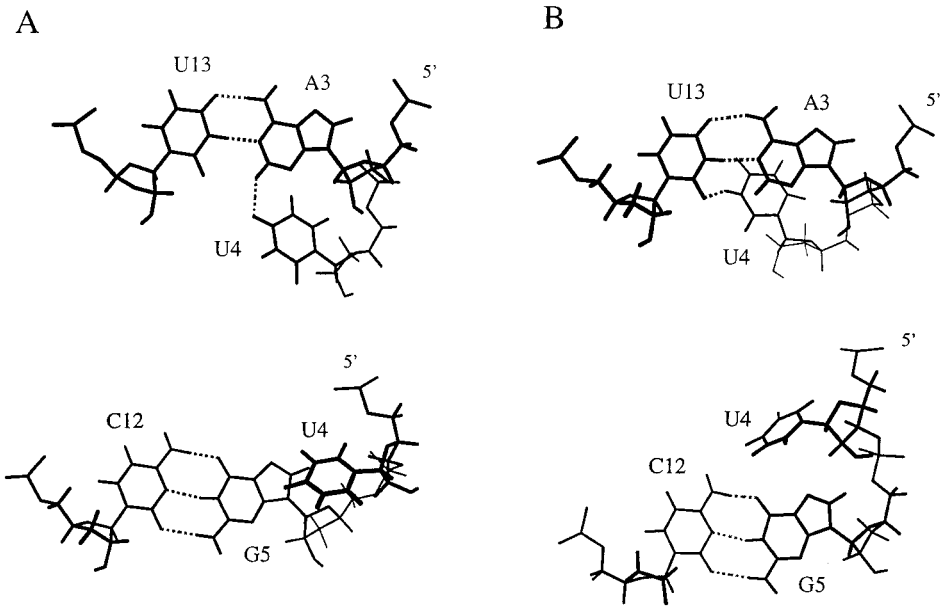

FIGURE 4 The projection of the bulge nucleotide U4 on the plane of the flanking basepairs at the 5′ side of the bulge (upper structure scheme) and the 3′ side of the bulge (lower structure scheme). (*A*) Bulge region in the structure belonging to the group *bul_in_1*. (*B*) Bulge region in the structure belonging to the group *bul_in_2*.

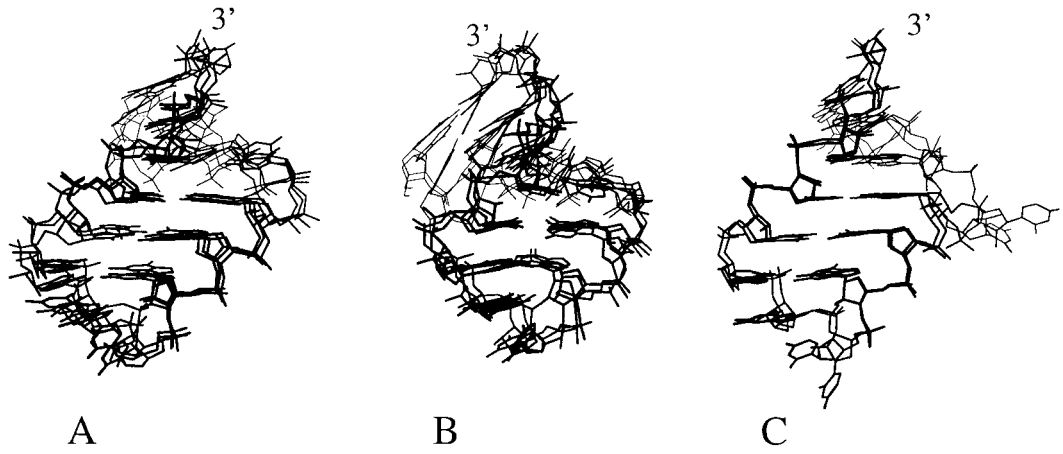

FIGURE 5 View of the superposition of the final structures (averaged over the last 20 ps of MD simulations) in the three groups. (*A*) Structures belonging to the group *bul_in_1* (Sb1, Ss3, Ss4). (*B*) Structures belonging to the group *bul_in_2* (Sb2, Ss5, Ss6). (*C*) Structures from the group *bulge_out* (Sb7, Sb8). View into the minor groove.

between bases in the loop (Sb2, Ss5a, Ss6) there is no (G7)N1-H. . .O1P(A10) hydrogen bond but the remaining three hydrogen bonds (G7)N2-H. . .N7(A10), (G7)N2-H. . .O1P(A10) and (G7)O2′-H. . .N7(G9) are stronger.

The angle between normal vectors of the bases G7 and A10, which indicates the relative orientation of the bases, is in the 20–30° range. The G7-A10 bases with a water bridge between them are closer to planarity than in the conformation without the water bridge.

We did not observe hydrogen bonds (G7)O2′-H. . .O6(G9) or (G7)O2′. . .H-N6(A10), identified in the NMR study of GNRA tetraloops (Jucker et al., 1996).

During all simulations, stacking between the G9 and A10 bases in the loop is well maintained. In most of the simulations we also found that U8, the second base in the loop, stacks with G9. In only one case, simulation Sb8, did we observe a transformation to an unstacked conformation. This transformation was connected with a change of the sugar pucker of nucleotide U8 and occurred after 640 ps of simulation.

TABLE 3 Angles between the vectors normal to the base planes calculated for basepairs A3-U13 and G5-C12 flanking bulge nucleotide and for the bases (bulge U4 and base U13) located in the opposite strand

	A3-U13	G5-C12	U4-U13	Group of structures
Sb1	23 (9)	13 (6)	29 (13)	*bul_in_1*
Ss3	27 (9)	12 (6)	28 (14)	
Ss4	30 (11)	12 (7)	23 (13)	
Sb2	34 (13)	16 (7)	36 (11)	*bul_in_2*
Ss5	35 (12)	15 (7)	45 (11)	
Ss6	28 (18)	41 (12)	28 (18)	
Sb7	19 (9)	13 (7)		*bul_out*
Sb8	17 (8)	12 (7)		

Angle values are in degrees. RMS fluctuations are given in parentheses.

The A10 and C11 bases do not stack except in the simulation Ss6. Hydrogen bonds between the 2′OH group of A10 and a phosphate oxygen of C11 were noticed during two simulations, Sb2 and Sb8 (Table 4).

Backbone torsion angle and sugar conformation transformations

In Table 6 the regions for the backbone torsion angles, which were different from A-form RNA, and their main transition events are shown. We do not discuss here transitions that took place during the initial 100 ps of simulation and were mostly of an equilibration nature connected with adopting new conformations different from the model built initial structure. Average torsion angles for the backbone fragments 1_2, 14_15 in the 5′ and 3′ends and for fragments 5_6_7, 9_10 have an A-form geometry in all structures independent of the bulge arrangement (n-1_n denotes backbone fragment $C3'_{n-1}$-$O3'_{n-1}$-P_n-$O5'_n$-$C5'_n$-$C4'_n$ defined by torsion angles ϵ_{n-1}, ξ_{n-1}, α_n, β_n, γ_n). We want to point out that the fragment 5_6_7, consisting of three subsequent guanosines, is very similar in all structures and shows the smallest fluctuations of the torsion angles during simulations. The 9_10 fragment belonging to the loop part also displays the A-form geometry.

Deviations from the A-form and differences between structures are found in the bulge region, in the loop region, and, for the *bulge_in* simulations, for the fragment opposite the bulge. In the bulge region for the *bulge_out* simulations the flexible fragment encompasses the backbone fragment 2_3_4_5 where several transitions took place (Table 2). For simulations *bulge_in* deviations from the A-form appear for the fragments 4_5 and 5_6, and during 600 ps of the production run no transitions were observed. In the loop part for the fragment 7_8, the backbone changes direction as a

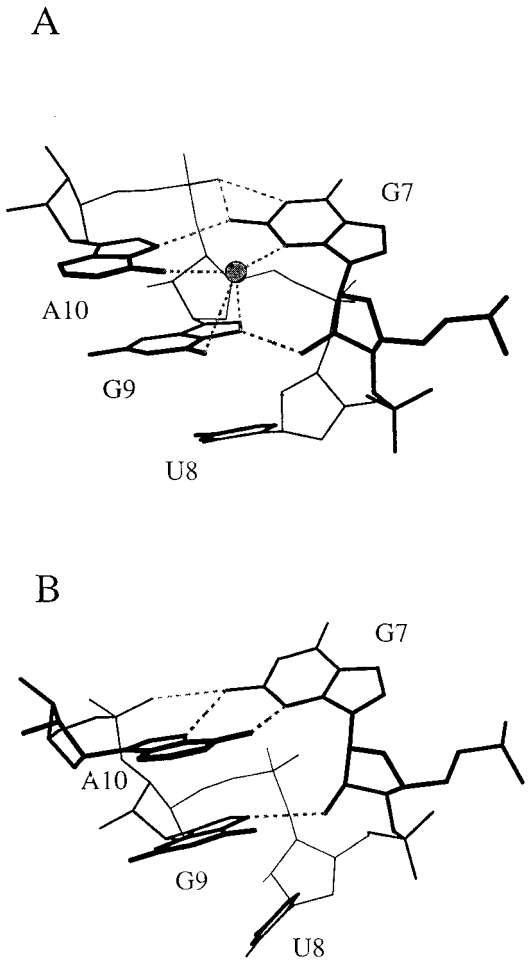

FIGURE 6 Hydrogen bonds observed in the tetraloop (nucleotides 7–10). (*A*) Structure containing the water molecule located inside the loop. (*B*) Structure without the internal water molecule.

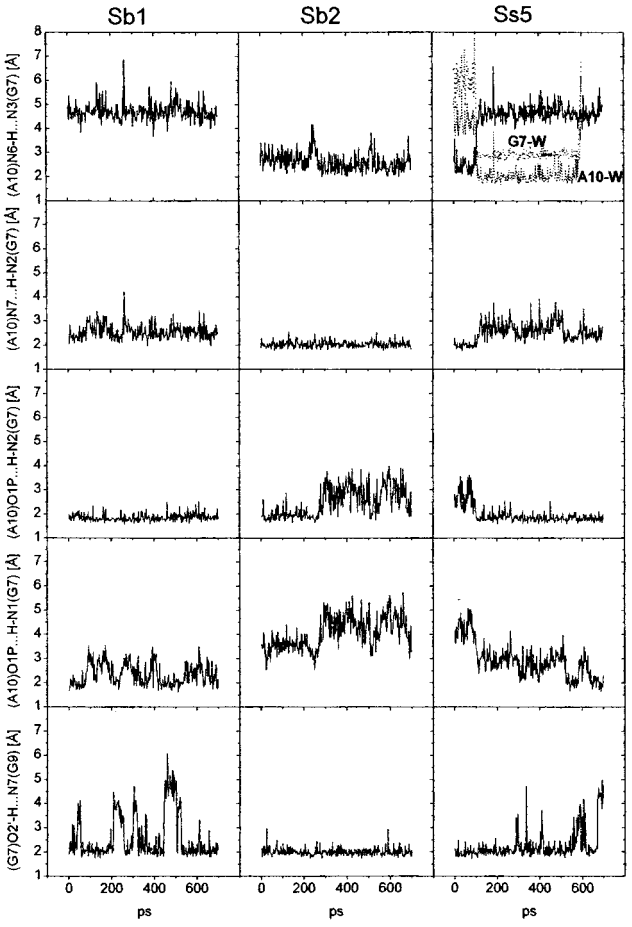

FIGURE 7 The time evolution of the hydrogen bonding distances in the tetraloop for simulations: Sb1 with water-mediated interaction between G7 and A10, Sb2 without bridging water, and Ss5 showing changes during creation of the water bridge, with the (G7)N7. . . Ow and (A10)N6-H. . . Ow hydrogen bonds indicated by G7-W and A10-W, respectively.

result of α_8 being in the +ap region and of a slight rotation of β_8 from the +ap region toward the border of the +ac/+ap region. During one simulation (Sb8), a transition of nucleotide U8 from stacking to unstacking conformation was observed. This transition involved a rotation of α_8 from +ap to +ac, a change of the sugar pucker from C3′-endo to C2′-endo and some changes in the ϵ_8, ζ_8, and α_9 torsion angles. An unstacked nucleotide in this position was observed in the NMR structure of a GCAA loop (Jucker et al., 1996). At step 8_9 only one structure, Ss4, differs from the A-form with α_9, β_9, and γ_9 in the +ac, −ac, and +ap region, respectively. Variability in the conformation of the backbone is observed at the A10:C11 step connecting the loop and the stem part. We observed three kinds of arrangement of the backbone torsion angles in this region. Conformations of the backbone with torsion angles different than in A-form result in a lack of stacking interactions between A10 and C11. Only during the Ss6 simulation do torsion angles for the backbone fragment 10_11 have A-form geometry, except for a temporary transition of the angles ϵ_{10}, ζ_{10}, α_{11}, and stacking between A10 and C11 is maintained. For all *bulge_in* structures the stem part opposite to the bulge (11_12_13_14) differs from the A-RNA structure. The γ torsion angle is found in the ap conformation for at least two of these nucleotides. For the *bulge_out* simulations the torsion angles for the strand 11_12_13_14 opposite the bulge appear in A-RNA geometry.

All structures display short distances between adjacent phosphate atoms P7-P8 (5.3–5.5 Å) and P6-P7 (5.4–5.7 Å), and there are water bridges between adjacent phosphate oxygen atoms in this fragment (J. Sarzynska, T. Kulinski, and L. Nilsson, manuscript in preparation). The remaining P_n-P_{n+1} distances differ between positions and simulations. This leads to differences in the hydration pattern.

In general, sugar units are in the C3′-endo puckering mode, as in a regular A-RNA helix. Most of the average values of the pseudorotation phase angle P are in the range of 0° to 18°. There are three regions where a transition from

TABLE 4 Average number of hydrogen bonds between 2′-OH group and RNA hydrogen bond acceptor

Simulation		*bul_in_1*			*bul_in_2*			*bul_out*	
Donor	Acceptor	Sb1	Ss3	*Ss4*	Sb2	Ss5	*Ss6*	Sb7	Sb8
G2-2′OH	O2P(A3)	–	–	–	–	–	–	0.99	0.25
A3-2′OH	O5′(U4)	0.63	0.53	0.44	–	–	–	–	–
	O4′(U4)	–	–	–	0.31	0.21	–	–	–
	O5′(G5)	–	–	–	–	–	–	0.30	–
U4-2′OH	O2P(G5)	–	–	–	–	–	–	–	0.24
G7-2′OH	N7(G9)	0.69	0.62	0.67	0.99	0.80	0.97	0.38	0.30
A10-2′OH	O2P(C11)	–	–	–	0.27	–	–	–	0.23
C11-2′OH	O5′(C12)	–	0.25	–	–	–	0.31	–	–
C12-2′OH	O5′(U13)	–	–	–	–	–	0.49	–	–

The average number of hydrogen bonds is calculated as the fraction of time during the simulation with a hydrogen bond present between the specified donor and acceptor. Criteria: distance D-H. . .A < 2.5 Å, angle D-H. . .A $> 135°$. Only hydrogen bonds with average number >0.2 are shown. The 2′O was not found as an acceptor for intramolecular hydrogen bonds.

the C3′-endo to the C2′-endo puckering was observed. In the bulge region we saw changing of the sugar pucker for the bulge nucleotide U4 and the preceding nucleotide A3 during the simulation *bulge_out*. In the 3′ strand opposite the bulge, sugar transformations took place for nucleotide C12 during the simulations *bulge_in*: one, Ss6, was not reversible to the C2′-endo, and one, Ss4, was reversible to C4′-exo. In the loop region only one transformation to the C2′-endo puckering was noticed for nucleotide U8 in the loop. Sugar puckering shifted to C2′-exo for nucleotides: G5 for *bulge_in_1* simulations, C11 for *bulge_out* simulations, and C12 for simulation Ss5. The glycosidic torsion angle about the C1′-N1 bond, χ, generally was in the range $-180°$ to $-144°$, corresponding to the anti region. Extreme values in this region were observed for $\chi 4$ (rotated toward $-144°$) and $\chi 5$ (rotated toward $-180°$). During a high fraction of the time of the *bulge_out* simulations, the $\chi 4$ angle was higher than $-120°$ and the $\chi 3$ angle was above $-130°$. In one case, for $\chi 13$ during the Ss6 *bulge_in* simulation, we saw a temporary rotation to the high anti ($-$sc) region (to about $-105°$).

Sugar conformation changes from C3′-endo to C2′-endo, sometimes reversible, were observed at the 3′ end in all simulations. For the G1-C15 terminal basepair, hydrogen bond breaking was observed only in one case, Ss3, after about 400 ps.

C-H. . .O contacts with C. . .O distances between 3.0 and 4.0 Å and C-H. . .O angles $>90°$ are considered as contributing to

TABLE 5 Hydrogen bond geometry in the tetraloop

	G7-A10				G7-G9
	Base-base		Base-phosphate oxygen		Ribose-base
	N3. . .H-N6	N2-H. . .N7	N2-H. . .O1P	N1-H. . .O1P	O2′-H. . .N7
Sb1	4.69 (0.38)	2.54 (0.31)	1.84 (0.15)	2.35 (0.45)	2.59 (0.92)
	160 (11)	141 (12)	158 (10)	139 (12)	147 (34)
Sb2	2.61 (0.29)	2.04 (0.15)	2.49 (0.62)	4.05 (0.46)	2.01 (0.16)
	161 (9)	160 (11)	139 (16)	120 (7)	162 (10)
Ss3	4.74 (0.35)	2.53 (0.32)	1.82 (0.14)	2.32 (0.47)	2.66 (0.98)
	159 (11)	141 (11)	158 (10)	140 (12)	142 (42)
Ss4	4.80 (0.53)	2.57 (0.40)	1.85 (0.15)	2.57 (0.40)	3.17 (1.47)
	162 (10.0)	142 (14.0)	157 (11)	137 (11)	121 (55)
Ss5*	2.51 (0.36)	1.99 (0.13)	2.65 (0.50)	4.19 (0.50)	1.95 (0.16)
	159 (11)	162 (9)	136 (13)	122 (7)	162 (9)
Ss5†	4.65 (0.32)	2.63 (0.34)	1.84 (0.15)	2.70 (0.49)	2.12 (0.28)
	162 (10)	144 (11)	168 (10)	132 (11)	154 (28)
Ss6	2.72 (0.37)	2.04 (0.16)	1.98 (0.19)	3.49 (0.34)	2.04 (0.17)
	164 (9)	156 (12)	150 (11)	122 (6)	162 (10)
Sb7	4.64 (0.26)	2.33 (0.20)	1.89 (0.15)	1.93 (0.16)	3.49 (1.33)
	162 (9)	139 (11)	152 (9)	150 (8)	107 (55)
Sb8	4.63 (0.35)	2.35 (0.25)	1.89 (0.15)	1.97 (0.24)	3.69 (1.36)
	162 (9)	140 (11)	154 (9)	149 (9)	100 (56)

Average distances (Å), on the first line for each simulation, and angles (degrees), on the second line for each simulation, from the whole trajectory (700 ps); rms fluctuations are given in parenthesis.

* From the period 0–108 ps.

† From the period 110–700 ps.

TABLE 6 Conformational ranges for the backbone torsion angles (Saenger, 1984) different than canonical A-form

Nucleotide	ϵ_{i-1}	ζ_{i-1}	α_i	β_i	γ_i	P_i	Simulation
			Bulge in				
4	−ap	−sc/−ac					Sb1, Ss3, Ss4
5			+ac	−ap/−ac	−ap		Sb1, Ss3, Ss4
	−ac/−ap		+ac		+ap/−ap	$C_{2'exo}$	Ss5
	−ac/−ap		−ac			$C_{3'endo}/C_{2'exo}$	Sb2, Ss6
8			+ap	+ac			all
9				−ac/+ap			Sb1, Ss3, Sb2, Ss5, Ss6
		−sc/−ac	+ac	−ac → −ap	+ap		s4
11	−ap	+sc	−ac	+sc/+ac	+ap/−ap		Sb1, Ss3, Ss4, Sb2, Ss5
	−ac ↔ +ap	−sc ↔ +sc	−sc ↔ −ac				Ss6
12	−ap		+ac		+ap/−ap	$C_{3'endo}/C_{2'exo}$	Sb1, Ss3, Ss5
	−ap		+ac		+ap/−ap	$C_{2'endo} \rightarrow C_{3'endo} \leftrightarrow C_{4'exo}$	Ss4
	−ap ↔ −ac	−sc/−ac ↔ −ap	+ap ↔ +ac	−ap ↔ ac	+ap/−ap	$C_{3'endo} \rightarrow C_{2'endo}$	Ss6
13			+ac		+ap/−ap		Sb1, Ss4, Sb2, Ss5, Ss6
			+ac				Ss3
14			+ac	−ac/−ap	−ap		all

Nucleotide	ϵ_{i-1}	ζ_{i-1}	α_i	β_i	γ_i	P_i	Simulation
			Bulge out				
3	+ac ↔ +sc	+sc ↔ +ac	−ap ↔ −sc	+ap/−a ↔ +ac		$C_{3'endo} \leftrightarrow C_{4'exo}$	Sb7
	+ac → −ac	+sc → −sc	−ac → −sc			$O_{4'endo} \rightarrow C_{2'endo}$	Sb8
4		+ap → ap/−ac	−ac → −ap/+ap	−ac → +ac/+ap		$C_{3'endo} \rightarrow C_{2'endo}$	Sb7
	−ac/−sc	−ac → −ac/−sc	+sc	+ac		$C_{3'endo} \leftrightarrow O_{4'exo}$	Sb8
5			+sc	+ac	−ap		Sb7
	−ac → −ap	+sc/+ac → +sc	+sc ↔ +ap	+ac → +ap	−ap → −sc		Sb8
8			+ap	+ac/+ap			Sb7
			+ap → +ac			$C_{3'endo} \rightarrow C_{2'endo}$	Sb8
9	−ac → −ac/−sc	−sc → −ac		+ac/+ap			Sb8
11			+ac	−ac	−ap/+ap	$C_{2'exo}$	Sb7
	+ap/+ac → −ac	+sc → −sc	+sc → +ac	−ac	−ap/+ap	$C_{2'exo}$	Sb8

Angles with no indicated range stay in the main conformation corresponding to the A-form geometry.
Torsion angle regions (Saenger, 1984): ±sp = 0° to ±30°, ±sc = ±30° to ±150°, ±ap = ±150° to ±180°.
The main conformation:
$-150° < \epsilon < -120°$ with a mean −141° (−ac region)
$-90° < \zeta < -60°$ with a mean −72° (−sc region)
$-90° < \alpha < -60$ with a mean −70° (−sc region)
$150° < \beta < 210°$ with a mean 175° (+ap region)
$50° < \gamma < 75°$ with a mean 59° (+sc region).

the stability of RNA (Wahl and Sundaralingam, 1997; Auffinger and Westhof, 1996). Base-backbone C(6/8)-H. . .O5′ interactions are frequently detected in the examined RNA. The geometry suitable for a C-H. . .O5′ interaction requires the γ torsion angle around C4′-C5′ bond in the region +sc, positioning the O5′ oxygen atom under the sugar ring and the base in the anti conformation, which is typical for A-RNA. In our simulations the C-H. . .O5′ contact is well correlated with the torsion angle γ. In all *bulge_in* simulations this contact is broken very often for nucleotides 11–14, nucleotide 5 next to the bulge and in one case for nucleotide 9. In *bulge_out* simulations it is not maintained for nucleotides 3, 4, and 5 in the bulge region and for nucleotide 11.

Another C-H. . .O short contact often found in RNA is from C2′-H to O4′ of the subsequent nucleotide. Generally this contact is weaker than C-H. . .O5′. In our simulations only the geometry in the turning point in the loop between nucleotides 7 and 8 is never suitable for the C2′-H. . .O4′ interaction between sugars. The other regions display more variability between structures, but this contact is often detected. The C2′-H. . .O4′ interaction is also destroyed due to the transformation of the sugar conformation from C3′-endo to the C2′-endo (simulation Ss6). The contact (U8)C5-H. . .O_2′(G7) in the loop meets the criteria for a C-H. . .O contact for over 50% of each trajectory.

Structural flexibility

To identify regions of high and low mobility in the structures, we calculated RMS fluctuations around the average structure for the last 200 ps of the trajectories. RMS fluctuations were averaged per nucleotide separately for the backbone and base atoms (Fig. 8). Of special interest for us was how the bulge nucleotide arrangement influences the dynamics of the whole structure. We found that nucleotides

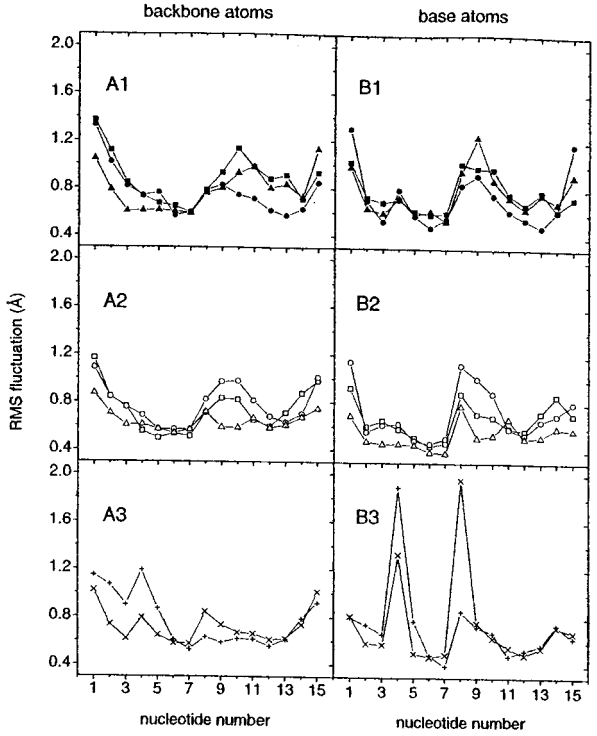

FIGURE 8 RMS fluctuations per nucleotide separate for the backbone atoms and the base atoms over the period 500–700 ps of the trajectory relative to their average positions. (*A1*) and (*B1*) Simulations giving structures belonging to *bulge_in_1* group: Sb1 *(solid square)*, Ss3 *(solid circle)*, Ss4 *(solid triangle)*. (*A2*) and (*B2*) Simulations giving structures belonging to *bulge_in_2* group: Sb2 *(open square)*, Ss5 *(open circle)*, Ss6 *(open triangle)*. (*A3*) and (*B3*) Simulations *bulge_out*: Sb7 *(cross +)*, Sb8 *(cross ×)*.

G6 and G7 show the lowest fluctuations both for the backbone and base atoms in all simulations. Nucleotide G5 in the *bulge_in* simulations is also characterized by low mobility. In fact, nucleotide G7 is the first tetraloop nucleotide. The following three nucleotides from the tetraloop (nucleotides 8–10) display relatively large fluctuations, and the base atoms of the nucleotide U8 fluctuate more than the backbone atoms. The stem part opposite to the bulge (nucleotides 11–14) displays lower fluctuations in comparison to the mobile part of the tetraloop, but some structures from the *bulge_in* group exhibit quite high backbone fluctuations. For the bulge nucleotide U4 we can clearly see a difference in the mobility between structures *bulge_in* and *bulge_out*. Backbone fluctuations for nucleotide 4 in structures from the *bulge_in* group are similar to that for the adjacent nucleotide G5, and fluctuations of the base atoms are slightly higher for structures from the *bulge_in_1* group than from the *bulge_out_2* group. However, backbone fluctuations for the bulge nucleotide U4 in the structures from the group *bulge_out* are higher than for flanking nucleotides with much higher base fluctuations. The largest motion amplitude was found for the terminal nucleotides, with higher fluctuations at the 5′ end.

Another way to provide insight into the atomic motions is to calculate the RMS fluctuations of the atom-atom distances. These calculations give us information about atom motions relative to the other atoms in the molecule. Of interest to us was the relative mobility of the backbone atoms. Fig. 9 displays examples of RMS fluctuations of the selected backbone atoms (P-O5′-C5′-C4′-C3′-O3′) from the last 200 ps of the trajectories. The graphs represent three groups of structures. In the graphs only small fluctuations are displayed (0.0–0.5 Å). Small fluctuations (darker areas in Fig. 9) between atoms from neighboring nucleotides indicate local rigidity of the backbone. The backbone in the bulge region in the simulations Sb1 and Sb2 is more rigid than during the simulation Sb7. The stem fragment opposite the bulge (nucleotides 11–15) is clearly more rigid for structures from the *bulge_out* than for the *bulge_in* group. In the loop part for nucleotides, which show relatively high fluctuations around average positions (U8, G9, A10), fluctuation of atomic distances, are not relatively higher. This means that the backbone itself in the loop region is relatively rigid with large fluctuations as a unit around an average position in space. The highest distance fluctuations took place between atoms from nucleotides 2 and 9 and are connected with the motion of the 5′ end relative to the tetraloop (data not shown).

In addition, the backbone flexibility has been analyzed by examination of the presence of conformational changes leading to structures with the $O_2'(i)\ldots P(i+1)\text{-}O5'(i+1)$ angle close to 180° and a short $O_2'(i)\ldots P(i+1)$ distance. Such an in-line conformation is believed to be necessary for ion-induced hydrolysis of the phosphodiester linkage (Brown et al., 1985). We did not observe spontaneous fluctuations toward the in-line conformation during the analysis of all phosphodiester linkages over 8 simulations. In our simulations the $O_{2i}'\ldots P_{i+1}'\text{-}O5_{i+1}$ distance and angle are centered on 4.0 Å and 75° respectively. The $O_{2i}'\ldots P_{i+1}'\text{-}O5_{i+1}$ angles were never larger than 155° and the O_2' never came closer than 3.05 Å to the cleavable phosphate. A small fraction of the conformations is characterized by angles in the region 100–155° (7%) and distances in the region 3.05–3.55 Å (3.6%). However, when analyzing particular linkages, we can see that some of them are better oriented for the cleavage reaction than others. Some angles and distances display a wide range of values due to conformational variability. One example of this is shown in Fig. 10. Linkage 4_5 in the flexible region is compared with linkage 6_7 in the rigid region during the two *bulge_out* simulations (Sb7, Sb8). The $O_{2i}'\ldots P_{i+1}'\text{-}O5_{i+1}$ angles for the 4_5 linkage are shifted to the highest values and the $O_{2i}'\ldots P_{i+1}$ distances display a wide range of accessible values.

Solvent accessible surface area

The solvent accessible surface area (ASA; Lee and Richards, 1971) was calculated using a spherical probe of radius

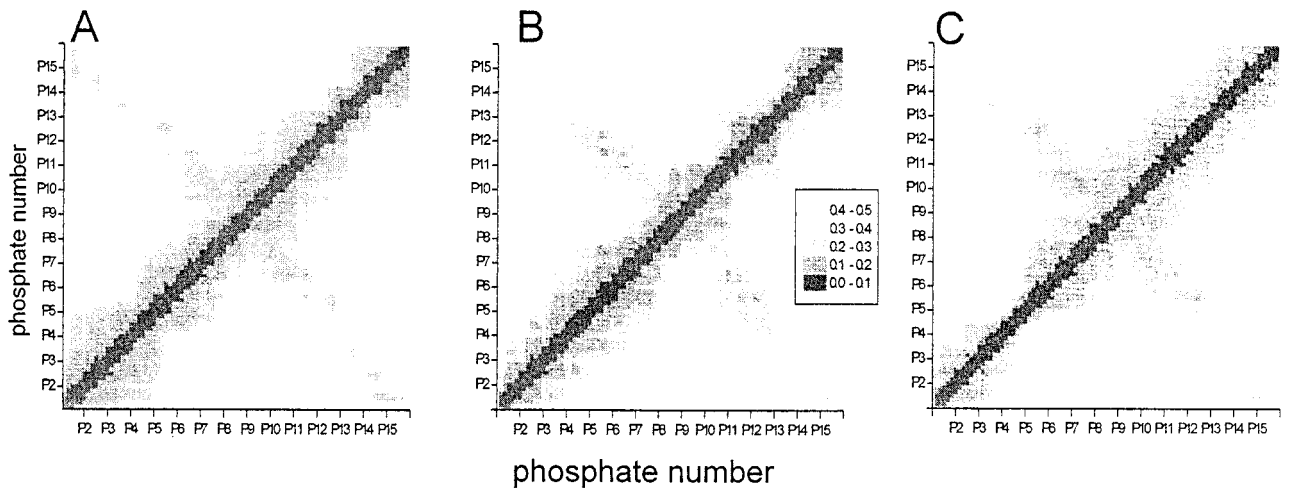

FIGURE 9 RMS fluctuations of the atom-atom distances for selected backbone atoms (atoms P-O5′-C5′-C4′-C3′-O3′) for the last 200 ps of trajectories. (*A*) Simulation Sb1 (*bulge_in_1*). (*B*) Simulation Sb2 (*bulge_in_2*). (*C*) Simulation Sb7 (*bulge_out*). Fluctuations in the range 0.0–0.5 Å are shown in a gradual scale as indicated in the legend. Darker squares correspond to lowest RMS fluctuation values.

1.4 Å corresponding to the radius of a water molecule. Average ASAs over trajectories for the RNA fragment from nucleotide 2 to 14 (without terminal nucleotides) are between 2442–2562 $Å^2$ with slightly higher values for the *bulge_out* simulations (Sb7, Sb8). The ASA of the studied RNA fragment is relatively stable throughout the MD simulations, with a standard deviation of 30–38 $Å^2$. The average ASA per nucleotide is in the range 188–197 $Å^2$. The contribution to the ASA from the backbone and bases is about 75% and 25%, respectively.

To see the differences between regions of the 5S rRNA fragment, the average ASAs for individual atoms were calculated. Fig. 11 shows ASAs for phosphate oxygens O1P and O2P in each nucleotide averaged separately over *bulge_in* and *bulge_out* trajectories. The ASA for the O1P and O2P atoms is slightly larger (from 5 to 15 $Å^2$) in the 3′ side for nucleotides 11 to 15 than in the 5′ side for nucleotides 2 to 8. The O1P and O2P atoms for nucleotides 9 and 10 in the loop part show relatively low accessibility to water. In the region 12–14 in addition, we observed an

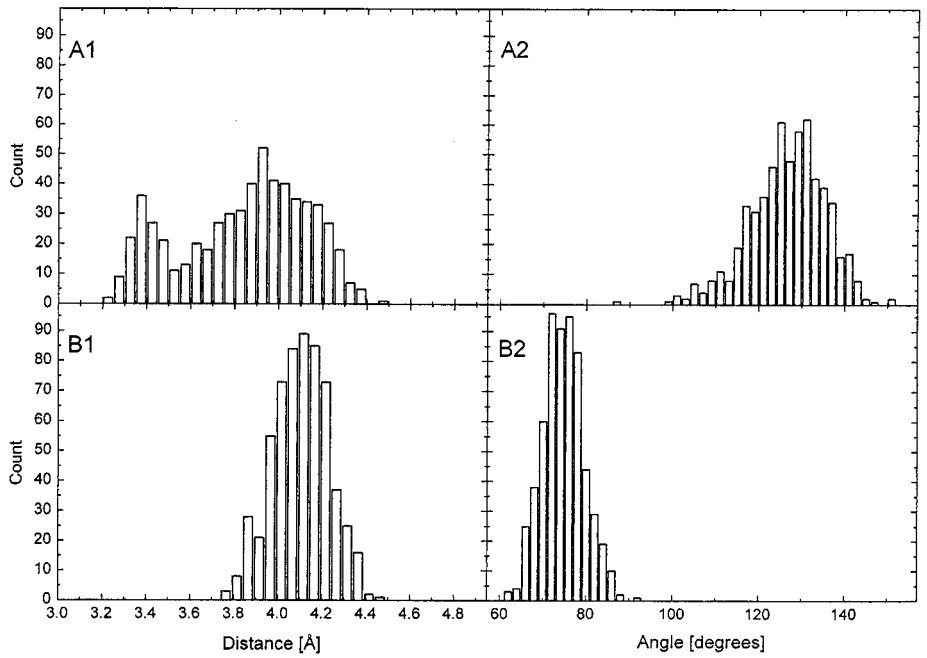

FIGURE 10 Histogram of the O'_{2i}. . . P_{i+1} distances and the O'_{2i}. . .P'_{i+1}-$O5_{i+1}$ angles for two nucleotides: U4 and G6 from simulations *bulge_out* (Sb7, Sb8).

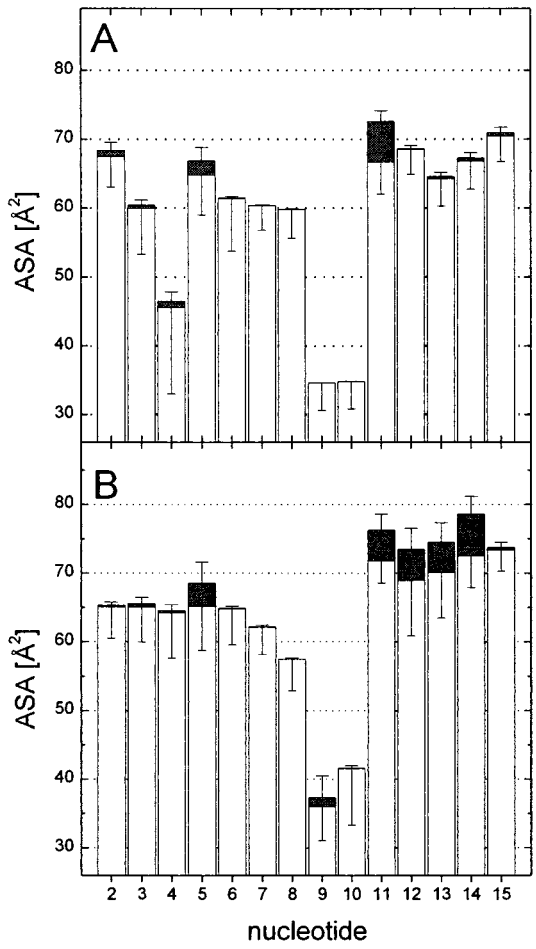

FIGURE 11 Solvent accessible surface area for O1P, O2P *(white columns)*, and O5′ *(gray columns)* atoms averaged over MD simulations. (*A*) Structures *bulge_in* averaged over six simulations, Sb1, Ss3, Ss4, Sb2, Ss5, and Ss6. (*B*) Structures *bulge_out* averaged over two simulations, Sb7 and Sb8.

increase of the ASA for the O5′ atoms. The ASA for the O5′ atoms is correlated with the backbone torsion angle γ around the C4′-O5′ bond. With γ in the +sc region, typical for A-RNA, the ASA of the O5′ atom is close to 0. When γ rotates to the ap region, the ASA for the O5′ atom increases by about 5 Å^2. This happens for most of the nucleotides 11–14 for *bulge_in* simulations, for nucleotide C11 only for *bulge_out* simulations, and for nucleotide G5 for all simulations.

DISCUSSION

The object of this study is a terminal part of one of the arms of 5S rRNA from wheat germ corresponding to the nucleotide sequence from 81 to 95 of helix IV - loop D (Fig. 1). The consensus secondary structure of this region consists of of a regular helix closed by a tetraloop. This region is characterized by the lowest free energy of the structure formation and was proposed as a center of the nucleation for 5S RNA folding (Kulinski et al., 1997).

Initial structures used for MD simulations were constructed manually according to a base-pairing scheme as proposed by (Kulinski et al., 1997) with structural motifs taken from structural databases. We assumed that the tetraloop sequence GCGA of loop D in the plant 5S rRNA forms the structure typical for a GNRA loop. The GNRA loops are a common motif in ribosomal RNA and their structures in solution were characterized by NMR (Jucker et al., 1996). A similar, characteristic structure was found in RNA molecules of different origin: hammerhead ribozyme (Pley et al., 1994), group I ribozyme (Cate et al., 1996; Kieft and Tinoco, 1997), leadzyme (Hoogstraten et al., 1998), sarcin/ricin loop from 28S rRNA (Szewczak and Moore, 1995; Correll et al., 1998, 1999). The unique known crystal structure of the D loop from bacterial 5S rRNA exhibits some differences in the tetraloop GCGA conformation in respect to the others previously described (Perbant et al., 1998).

In general, the information about the structure of single pyrimidine bulges in RNA is limited. In an early NMR study a uridine bulge was found in an extra-helical conformation (van den Worm et al., 1998). A more recent NMR study reveals a cytosine bulge located outside the helix in the iron response element (IRE) RNA where the cytosine bulge makes specific interactions with IRE protein (Addes et al., 1997; Gdaniec et al., 1998) and in the HIV-1 genomic RNA (Puglisi and Puglishi, 1998).

Single adenosine bulges in RNA were studied more extensively. From the x-ray study of a viral coat protein/RNA complex, the adenosine bulge is outside the helix (Valegård et al., 1997; van den Worm et al., 1998). However, the NMR study of the RNA binding sequence for the coat protein bacteriophage R17 reveals the adenosine bulge inside the helix (Borer et al., 1995). In the crystal structure of a hybrid DNA/RNA the adenosine bulge is located outside the helical track (Portmann et al., 1996). Single purine bulges, where the bulged nucleotide was a 2-aminopurine, a fluorescent adenosine analogue, were studied using time-resolved spectrofluorimetry. The results point to the coexistence of two conformational states: one with 2-aminopurine looped out of the helix, and another where the bulged base is stacked within helix (Kulinski et al., 1996).

For that reason, we have built two initial models: in one structure the bulge was modeled inside, and in the other outside the helix. We used them to examine the stability of both configurations and their influence on the rest of the structure. To improve conformational sampling in the simulations, we carried out several trajectories for each of the initial structures with different initial conditions rather than a single long trajectory. The resulting structures kept the initial general bulge orientation and differed mainly in the bulge accommodation and the conformation of the stem part opposite the bulge. No tendency to continuous migration of the intrahelical U base toward the outside of the helix, nor

in the reversed direction, was observed in any trajectory, indicating that there is a free energy barrier for this transition. From the present trajectories it is not possible to estimate neither the size of the barrier, nor the free energy difference between the two types of conformation. Structures with the bulge inside can be divided into two groups according to the position of the bulge nucleotide U4 relative to the flanking basepairs. For the structures with the bulge outside the helix a high backbone flexibility was observed in the bulge region.

Zacharias and Sklenar (1999) applied a hierarchical method and energetic evaluation with a continuum solvent model for the conformational analysis of the bulge nucleotide. This method was based on the assumption that the main conformational distortion in the double helix due to the bulge encompasses only the bulge nucleotide and nucleotides directly flanking the bulge side.

In our study, the way in which the bulge nucleotide is accommodated into the helix affected the stem part opposite the bulge. In this region the backbone conformation is extended. Also a sequence of the stem fragment contributes to the difference in stability between the 5′ and the 3′ sides. In the 5′ strand there are successive purines and in the 3′ strand successive pyrimidines. The purines stack better than pyrimidines (Saenger, 1984), which, on the one hand, makes the 3′ strand less rigid; on the other hand, this sequence seems to be more susceptible to the conformational changes due to bulge accommodation.

Our results concerning the loop part are in agreement with what has been obtained up to now. The 200-ps-long MD simulation of the GCAA tetraloop performed by Zichi (1995) shows a good agreement of the structural features derived from simulation with the NMR data. In that simulation the formation of water-mediated hydrogen bonds between the bases of the sheared G-A basepair in the tetraloop was observed. The GUGA tetraloop as a part of a hammerhead ribozyme was investigated by MD by Hermann et al. (1998). We have shown that the tetraloop can be stabilized by a network of hydrogen bonds, which is dynamic and is maintained even when some conformational rearrangements take place. In our simulations we observed a direct as well as water-mediated N6-H. . .N3 hydrogen bond between bases G7 and A10 in the tetraloop. We also observed transitions from an arrangement with a direct hydrogen bond to an arrangement with a water-mediated bridge.

The structure of two plant 5S rRNA species has been studied by nonspecific lead-induced hydrolysis (Ciesiolka and Krzyzosiak, 1996). This method is considered to be sensitive to the secondary structure (Ciesiolka et al., 1998; Zagorowska et al., 1998). The 5S rRNA fragment that was the subject of that study displayed a relatively weak cleavage on both sides of the bulge nucleotide U4 and in the region spanning nucleotides U8 and C12.

For the Pb^{2+}-dependent hydrolysis of the RNA backbone, the mechanism of intramolecular phosphoester transfer has been proposed (Zhou and Taira, 1998). Such a reaction involves a nucleophilic attack of the 2′O oxygen on the adjacent phosphorus center and the production of a transient 2′-3′ cyclic phosphate and 5′-OH terminus. It is believed that susceptibility to Pb^{2+}-induced hydrolysis of the polynucleotide chain is determined by its flexibility and the ability to adopt an in-line conformation (Ciesiolka, 1999). For that reason, the static structure model is not sufficient to explain the experimental cleavage pattern and a dynamic study can provide more useful information.

We can see some correlation between the dynamics of our models and the cleavage pattern. Experiments show a lack of lead induced cleavage at the three guanosine nucleotides from G5 to G7 (Ciesiolka and Krzyzosiak, 1996). In our simulations this fragment appears as the most rigid part of the molecule. In all structures independent of the bulge arrangement, this fragment kept a classical A-RNA conformation, and in this region we did not observe any transitions for the backbone torsion angles. This fragment also shows the lowest RMS atomic fluctuations around the average positions of the atoms. The region opposite the bulge is where the cleavage is observed. For this region we have found more possible conformations, and several changes of the conformations during the course of the simulations were observed (rotations of the torsion angles). Rotation of the γ backbone torsion angle from region +sc to ap causes loss of C-H. . .O contacts, which normally stabilize the structure, and increases the solvent exposure of O5′.

Soukup and Breaker (1999) observed a correlation between the spontaneous RNA cleavage rate and the in-line fitness of the nucleotide linkage. The conformational change that takes place at the cleavage site of the hammerhead ribozyme during self-cleavage was captured using x-ray crystallography (Murray et al., 1998). An MD study of the hammerhead ribozyme showed that inducing a flip of the ribose pucker from C3′-endo to C2′-endo at the ribose which holds the cleavable phosphate moved a linkage to in-line conformation (Hermann et al., 1998). That study suggested that conformational change at the cleavage site, which takes place during the hydrolysis, can be induced by transition in the sugar pucker.

In the course of our simulations we did observe spontaneous transitions of the sugar pucker. These transitions occurred in the sites susceptible to lead ion-induced hydrolysis. We have not observed spontaneous formation of the in-line conformation, but from the analysis of the $O_2'(i)$. . . P(i + 1)-O5′(i + 1) angles and $O_2'(i)$. . .P(i + 1) distances, differences in the accessible conformation between cleavage susceptible linkages and resistant linkages can be noticed.

The present simulations compare internal interactions and flexibility of the various regions of the models with the bulge localized inside the helix and the bulge pointing out

from the helix. Our study does not definitively answer the question of whether the bulge base is stacked into the helix or remains outside. The two forms may exist in an equilibrium: the structure model with the bulge inside the helix better explains the cleavage observed in the part of the stem opposite the bulge than the model with the bulge outside, whereas the flexible backbone in the bulge region observed for the structures with the bulge outside the helix can explain cleavage localized in this part of the structure.

This work was supported by the Swedish Institute, the Swedish Natural Science Research Council, the Magnus Bergvall Foundation, and the Swedish Research Council for Engineering Sciences.

REFERENCES

Addess, K. J., J. B. Basilion, R. D. Klausner, T. A. Rouault, and A. Pardi. 1997. Structure and dynamics of the iron responsive element RNA: implications for binding of the RNA by iron regulatory binding proteins. *J. Mol. Biol.* 274:72–83.

Arnott, S., P. J. C. Smith, and R. Chandrasekaran. 1976. Atomic coordinates and molecular conformations for DNA-DNA, RNA-RNA and DNA-RNA helices. *In* CRN Handbook of Biochemistry and Molecular Biology: Nucleic Acids. G. D. Fasman, editor. Cleveland, OH. 411–22.

Auffinger, P., and E. Westhof. 1996. H-Bond stability in the tRNA Asp anticodon hairpin: 3 ns of multiple molecular dynamic simulations. *Biophysical J.* 71:940–954.

Ban, N., P. Nissen, J. Hansen, M. Capel, P. B. Moore, and T. Steitz. 1999. Placement of protein and RNA structures into a 5 Å -resolution map of the 50S ribosomal subunit. *Nature.* 400:841–847.

Betzel, Ch., S. Lorenz, J. P. Furste, R. Bald, M. Zhang, Th. R. Schneider, K. S. Wilson, and V. A. Erdman. 1994. Crystal structure of domain A of *Thermus flavus* 5S rRNA and the contribution of water molecules to its structure. *FEBS Lett.* 351:159–164.

Borer, P. N., Y. Lin, S. Wang, M. W. Roggenbuck, J. M. Gott., O. C. Uhlenbeck, and I. Pelczer. 1995. Proton NMR and structural features of a 24-nucleotide RNA hairpin. *Biochemistry.* 34:6488–6503.

Brooks, III, C. L., and M. Karplus. 1983. Deformable stochastic boundaries in molecular dynamics. *J. Chem. Phys.* 79:6312–6325.

Brooks, B. R., R. E. Bruccoleri, B. D. Olafson, D. J. States, S. Swaminathan, and M. Karplus. 1983. CHARMM: a program for macromolecular energy, minimization, and dynamics calculations. *J. Comp. Chem.* 4:187–217.

Brown, R. S., J. C. Dewan, and A. Klug. 1985. Crystallographic and biochemical investigation of the lead(II)-catalyzed hydrolysis of yeast phenylalanine tRNA. *Biochemistry.* 24:4785–801.

Cate, J. H., A. R. Gooding, E. Podell, K. Zhou, B. L. Golden, C. E. Kundrot, T. R. Cech, and J. A. Doudne. 1996. Crystal structure of group I ribozyme domain: principles of RNA packing. *Science.* 273: 1678–1685.

Ciesiolka, J. 1999. Metal-ion induced cleavages in probing of RNA structure. *In* RNA Biochemistry and Biotechnology. J. Barciszewski and F. C. Clark, editors. Dordrecht, Boston, London.

Ciesiolka, J., and W. J. Krzyzosiak. 1996. Structural analysis of two plant 5S rRNA species and fragments thereof by lead-induced hydrolysis. *Biochem. Mol. Biol. Int.* 39:319–328.

Ciesiolka, J., D. Michalowski, M. Wrzesinski, J. Krajewski, and W. J. Krzyrzosiak. 1998. Patterns of cleavages induced by lead ions in different RNA secondary structure motifs. *J. Mol. Biol.* 275:211–220.

Clemons, W., Jr., J. L. May, B. T. Wimberly, J. P. McCutcheon, M. S. Capel, and V. Ramakrishnan. 1999. Structure of a bacterial 30S ribosomal subunit at 5.5 Å resolution. *Nature.* 400:833–840.

Correll, C. C., B. Freeborn, P. B. Moore, and T. A. Steitz. 1997. Metals, motifs, and recognition in the crystal structure of a 5S rRNA domain. *Cell.* 91:705–712.

Correll, C. C., A. Munishkin, Y.-L. Chan, Z. Ren, I. G. Wool, and T. A. Steitz. 1998. Crystal structure of the ribosomal RNA domain essential for binding elongation factors. *Proc. Natl. Acad. Sci. USA.* 95: 13436–13441.

Correll, C. C., I. G. Wool, and A. Munishkin. 1999. The two faces of the *Escherichia coli* 23 S rRNA sarcin/ricin domain: the structure at 1.11 Å. *J. Mol. Biol.* 292:275–287.

Dallas, A., and P. B. Moore. 1997. The loop E-loop D region of *Escherichia coli* 5S rRNA: the solution structure reveals an unusual loop that may be important for binding ribosomal proteins. *Structure.* 5:1639–1653.

Gdaniec, Z., H. Sierzputowska-Gracz, and E. C. Theil. 1998. Iron regulatory element and internal/bulge structure for ferrin mRNA studied by cobalt(III) hexamine binding, molecular modeling, and NMR spectroscopy. *Biochemistry.* 37:1505–1512.

Hermann, T., P. Auffinger, and E. Westhof. 1998. Molecular dynamics investigations of hammerhead ribozyme RNA. *Eur. Biophys. J.* 27: 153–165.

Hoogstraten, C. G., P. Legault, and A. Pardi. 1998. NMR solution structure of the lead-dependent ribozyme: evidence for dynamics in RNA catalysis. *J. Mol. Biol.* 284:337–350.

Joachimiak, A., M. Nalaskowska, M. Barciszewska, J. Barciszewski, and T. Mashkova. 1990. Higher plant 5S rRNAs share common secondary and tertiary structure: a new three domains model. *Int. J. Biol. Macromol.* 12:321–327.

Jorgensen, W. L., J. Chandrasekhar, J. D. Madura, R. W. Impey, and M. L. Klein. 1983. Comparison of simple potential functions for simulating liquid water. *J. Chem. Phys.* 1479:926–935.

Jucker, F. M., H. A. Heus, P. F. Yip, E. H. M. Moors, and A. Pardi. 1996. A network of heterogeneous hydrogen bonds in GNRA tetraloops. *J. Mol. Biol.* 264:968–980.

Kieft, J. F., and I. Tinoco, Jr. 1997. Solution structure of a metal-binding site in the major groove of RNA complexed with cobalt (III) hexammine. *Structure.* 5:713–721.

Kraulis, P. J. 1991. MOLSCRIPT: a program to produce both detailed and schematic plots of protein structures. *J. Appl. Crystallogr.* 24:946–950.

Kulinski, T., L. Bielecki, I. Zagorowska, and R. W. Adamiak. 1996. Introductory data on dynamics of RNA bulge duplexes: 2-aminopurine labelled loops. *Collect. Czech. Chem. Commun.* 61:265–267.

Kulinski, T., M. D. Bratek-Wiewiorowska, A. Zielenkiewicz, and W. Zielenkiewicz. 1997. Mg^{+2} dependence of the structure and thermodynamics of wheat germ and lupin seeds 5S rRNA. *J. Biomed. Struct. Dyn.* 14:495–507.

Lee, B., and F. M. Richards. 1971. The interpretation of protein structures: estimation of static accessibility. *J. Mol. Biol.* 55:379–400.

Lorentz, S., C. Betzel, E. Raderschall, Z. Dauter, and V. A. Erdmann. 1991. Crystallization and preliminary diffraction studies of 5S rRNA from the thermophilic bacterium *Thermus flavus*. *J. Mol. Biol.* 219:399–402.

MacKerell, A. D., J. Wiorkiewicz-Kuczera, and M. Karplus. 1995. An all-atom empirical function for the simulation of nucleic acids. *J. Am. Chem. Soc.* 117:11946–11975.

Murray, J. B., D. P. Turvey, L. Maloney, A. Karpeisky, Usman. N., L. Beilgeman, and W. G. Scott. 1998. The structural basis of hammerhead ribozyme self-cleavage. *Cell.* 92:665–673.

Norberg, J., and L. Nilsson. 2000. On the truncation of long-range electrostatic interactions in DNA. *Biophys. J.* (in press)

Perbant, M., A. Notle, S. Lorenz, R. Bald, C. Bezel, and V. A. Erdman. 1998. Crystal structure of domain E of Thermus flavus 5S rRNA: a helical RNA structure including a hairpin loop. *FEBS Lett.* 429:211–215.

Pley, H. W., K. M. Flaherty, and D. B. McKay. 1994. Three-dimensional structure of a hammerhead ribozyme. *Nature.* 372:68–74.

Portmann, S., S. Grimm, C. Workman, N. Usman, and M. Egli. 1996. Crystal structures of A-form duplex with single-adenosine bulges and a conformational basis for site-specific RNA self-cleavage. *Chem. Biol.* 3:173–184.

Puglisi, E. V., and J. D. Puglishi. 1998. HIV-1 A-rich RNA loop mimics the tRNA anticodon structure. *Nat. Struct. Biol.* 5:1033–1036.

Ryckaert, J.-P., G. Ciccotti, and H. J. C. Berendsen. 1977. Numerical integration of the cartesian equation of motion of a system with constraints: molecular dynamics of n-alcanes. *J. Comp. Phys.* 23: 327–341.

Saenger, W. 1984. Priciples of Nucleic Acid Structure. Springer-Verlag, New York.

Soukup, G. A., and R. R. Breaker. 1999. Relationship between internucleotide linkage geometry and the stability of RNA. *RNA.* 5:1308–1325.

Specht, T., J. Wolters, and V. A. Erdmann. 1990. Compilation of 5S rRNA and 5S rRNA gene sequences. *Nucleic Acids Res.* 18(suppl):2215–2230.

Stoldt, M., J. Wohnert, O. Ohlenschlager, M. Gorlach, and L. R. Brown. 1999. The NMR structure of the 5S rRNA E-domain-protein L25 complex shows preformed and induced recognition. *EMBO J.* 18: 6508–6521.

Steinbach, P. J., and B. R. Brooks. 1994. New spherical-cutoff methods for long-range forces in macromolecular simulation. *J. Comp. Chem.* 15: 667–683.

Szewczak, A. A., and P. B. Moore. 1995. The sarcin/ricin loop, a modular RNA. *J. Mol. Biol.* 247:81–98.

Szymanski, M., M. Z. Barciszewska, J. Barciszewski, and V. A. Erdmann. 1999. 5S Ribosomal RNA data bank. *Nucleic Acid Res.* 27:158–160.

Valegård, K., J. B. Murray, N. J. Stonehouse, S. van den Worm, P. G. Stockley, and L. Liljas. 1997. The three-dimensional structures of two complexes between recombinant MS2 capsids and RNA operator fragments reveal sequence-specific protein-RNA interactions. *J. Mol. Biol.* 270:724–738.

van den Worm, S. H. E., N. J. Stoehouse, K. Valegård, J. B. Murray, Walton, C., K. Frodborg, Stockley, P. G., and L. Liljas. 1998. Crystal structures of MS2 coat protein mutants in complex with wild-type RNA operator fragments. *Nucleic Acids Res.* 26:1345–1351.

Wahl, M. C., and M. Sundaralingam. 1997. C-H. . . O hydrogen bonding in biology. *Trends Biochem. Sci.* 22:97–102.

Wimberly, B., G. Varani, and I. Tinoco. 1993. The conformation of loop E of eukariotic 5S Ribosomal RNA. *Biochemistry.* 32:1078–1087.

Zacharias, M., and H. Sklenar. 1999. Conformational analysis of single-base nucleotide bulges in A-form DNA and RNA using a hierarchical approach and energetic evaluation with continuum solvent model. *J. Mol. Biol.* 289:261–275.

Zagorowska, I., S. Kuusela, and H. Löndberg. 1998. Metal ion-depended hydrolysis of RNA phosphodiester bonds within hairpin loops: a comparative kinetic study on chimeric ribo/2′-O-methylribo oligonucleotides. *Nucleic Acids Res.* 26:3392–3396.

Zhou, D.-M., and K. Taira. 1998. The hydrohysis of RNA: from theoretical calculation to the hammerhead ribosime-mediated cleavage of RNA. *Chem. Rev.* 98:991–1026.

Zichi, D. A. 1995. Molecular dynamics of RNA with the OPLS force field. aqueous simulation of a hairpin containing a tetranucleotide loop. *J. Am. Chem. Soc.* 117:2957–2969.